Non-Hermitian ring laser gyroscopes with enhanced Sagnac sensitivity

https://doi.org/10.1038/s41586-019-1780-4

Received: 10 April 2019

Accepted: 4 September 2019

Published online: 4 December 2019

Mohammad P. Hokmabadi¹, Alexander Schumer^{1,2}, Demetrios N. Christodoulides¹ & Mercedeh Khaiavikhan^{1,3}*

Gyroscopes are essential to many diverse applications associated with navigation. positioning and inertial sensing¹. In general, most optical gyroscopes rely on the Sagnac effect—a relativistically induced phase shift that scales linearly with the rotational velocity^{2,3}. In ring laser gyroscopes (RLGs), this shift manifests as a resonance splitting in the emission spectrum, which can be detected as a beat frequency⁴. The need for ever more precise RLGs has fuelled research activities aimed at boosting the sensitivity of RLGs beyond the limits dictated by geometrical constraints, including attempts to use either dispersive or nonlinear effects^{5–8}. Here we establish and experimentally demonstrate a method using non-Hermitian singularities, or exceptional points, to enhance the Sagnac scale factor⁹⁻¹³. By exploiting the increased rotational sensitivity of RLGs in the vicinity of an exceptional point, we enhance the resonance splitting by up to a factor of 20. Our results pave the way towards the next generation of ultrasensitive and compact RLGs and provide a practical approach for the development of other classes of integrated sensor.

Sensing involves the detection of the signature that a perturbing agent leaves on a system. In optics and many other fields, resonant sensors are made to be as lossless as possible so as to exhibit high quality factors¹⁴⁻¹⁷. As a result, their response is governed by standard perturbation theory, suited for loss-free or Hermitian arrangements¹⁵. Recently, however, there has been a growing realization that non-Hermitian systems biased at exceptional points (EPs)^{18,19,20}, can react much more drastically to external perturbations 9,10,21. This EP-enhanced sensitivity a direct byproduct of Puiseux generalized expansions—is fundamental by nature. In particular, for a system supporting an Nth-order EP, where Neigenvalues coalesce and their corresponding eigenvectors collapse on each other, the reaction to a perturbation (ϵ) is expected to follow an Nth-root behaviour $(e^{1/N})$. This is in stark contrast to Hermitian systems, where the sensing response is at best of order ϵ . Given that $\epsilon^{1/N} \gg$ ϵ for $|\epsilon| \ll 1$, this opens up new possibilities for designing ultrasensitive sensors based on such non-Hermitian spectral singularities 9-11. For illustration purposes, Fig. 1 provides a comparison between the eigenvalue surfaces associated with a Hermitian (Fig. 1a) two-level system (N=2) and its corresponding non-Hermitian counterpart (Fig. 1b) when plotted in a two-parameter space around their corresponding spectral degeneracies. As shown in Fig. 1b, the presence of an EP forces the two Riemann manifolds to become strongly intertwined with each other—an attribute that could in turn be used to enhance the performance of a sensor22

Given that sensing is important in many fields, the emerging idea of boosting the sensitivity of a particular system via non-Hermitian degeneracies could have substantial ramifications across several technical areas. Here, we show that the sensitivity of a standard helium-neon (He-Ne) RLG can be drastically enhanced provided that its resonator is judiciously modified so as to support an EP. Figure 2 depicts a schematic of the non-Hermitian RLG used in this study. As opposed to a standard RLG, the retrofitted cavity involves a Faraday rotator (FR) and a half-wave plate (HWP). These two elements, acting in conjunction with the Brewster windows (BW) incorporated on both ends of the He-Ne gain tube, can be used to introduce a differential loss contrast (or gain contrast), Δy , between the clockwise (CW) and the counterclockwise (CCW) lasing modes. The method used to achieve this is depicted in Fig. 2a, where the evolution of the state of the polarization associated with the two counter-rotating modes is provided at three consecutive points (A. B. C) in the cavity. In this arrangement, the BWs allow only x-polarized light to circulate in the cavity while rejecting the v component. As a result, the CW mode enters the FR as x-polarized at point A. Because of the magneto-optic effect, the polarization subsequently rotates by a small angle α (point B). Under the action of the HWP, the angle between the linear electric-field component and the preferred x axis is $2\beta - \alpha$ (point C), where the small angle β denotes the orientation of the fast axis of the HWP with respect to the x-y coordinate system. On the other hand, because of non-reciprocity, although the CCW mode also starts as x-polarized at point C, it exits at an angle of $2\beta + \alpha$ with respect to the x axis (point A) after traversing the same two optical components. Therefore, as clearly indicated in Fig. 2a, the CW mode is expected to experience lower losses than its CCW counterpart does, after passing through the BWs of the He-Ne tube. Hence, a differential loss (Δy) can be introduced between these two counterrotating modes. Finally, to establish an EP in this cavity, it is necessary to counteract this differential loss with a mode-coupling process²². In our system, the coupling between the CW and CCW modes is readily induced using a weakly scattering object (for example, an etalon), as shown in Fig. 2a. The aforementioned processes can be formally described by employing a Jones calculus approach for the elements

1CREOL, The College of Optics and Photonics, University of Central Florida, Orlando, FL, USA. 2Institute for Theoretical Physics, Vienna University of Technology (TU Wien), Vienna, Austria. ³Ming Hsieh Department of Electrical and Computer Engineering, University of Southern California, Los Angeles, CA, USA, *e-mail: khaiayik@usc.edu

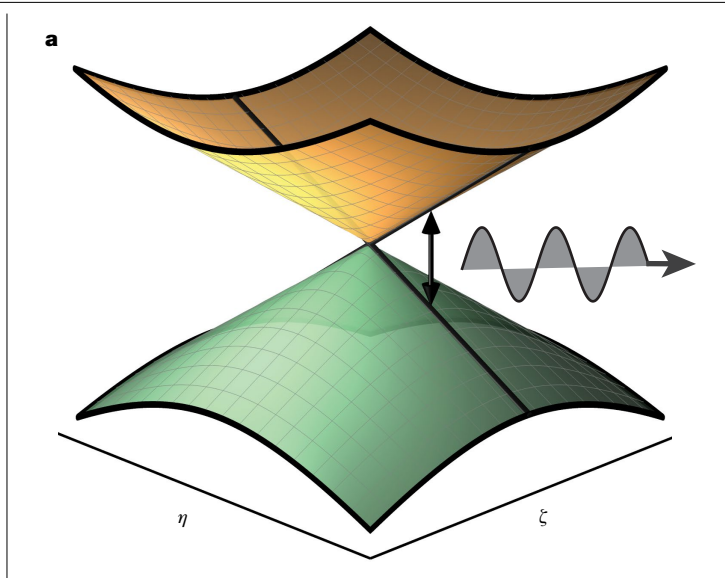
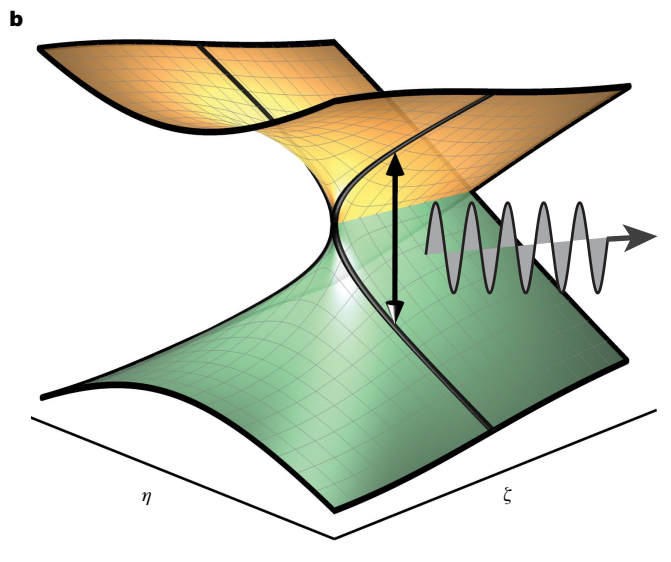


Fig. 1 | Conceptual illustrations comparing the eigenvalue surfaces associated with Hermitian and non-Hermitian two-level systems. a, The real part of the eigenvalues plotted in parameter space $(n-\zeta)$: normalized detuning. η , versus normalized coupling/gain-loss contrast, ζ) when the arrangement is Hermitian. Because of the Hermiticity, this system responds linearly to



perturbations. b, The real part of the eigenfrequency surface corresponding to a non-Hermitian configuration in the same parameter space. In the presence of an EP, the two Riemann manifolds are strongly intertwined, leading to a squareroot response to perturbations, as indicated by the frequency of the emitted signal. Using this system, an enhanced sensitivity to small changes is expected.

involved (HWP, FR, BW, scattering object), where the polarization state of the CW and CCW waves can be monitored after each pass through the following transfer matrix $T = S_{SC} \times P \times J_{HWP} \times J_{FR} \times J_{BW}$ (see Supplementary Information). In this expression, S_{SC} represents a conservative scattering matrix (producing coupling) and P denotes a phase accumulation matrix that can in principle account for the Sagnac shift³. The matrices J_{HWP} , J_{FR} and J_{BW} are the respective Jones matrices describing the change of polarization after each element 23,24 .

To experimentally demonstrate this enhanced Sagnac sensitivity, we use a custom-made, educational-grade He-Ne RLG (purchased from Luhs; https://luhs.de/lm-0600-hene-laser-gyroscope.html). The triangular cavity has a length of 138 cm and supports a free spectral range of about 216 MHz at 632.8 nm. The maximum loss that can be afforded in this system is approximately 3.6%. This resonator is then retrofitted with a terbium gallium garnet (TGG) Faraday element that can provide up to about 4° rotation at a magnetic induction of about 80 mT. This is used in conjunction with a HWP with a rotation angle that can vary in a controlled manner with a resolution of 0.005°. An etalon in the cavity promotes lasing in a specific longitudinal mode while providing some level of coupling between the CW and CCW modes. Other elements, such as the TGG, also contribute to this coupling. Overall, the system is designed to allow maximum tunability in establishing an EP.

Figure 2b, c provides a comparison between the principles of operation of a standard RLG and the EP-based RLG arrangement used in this study. In the former configuration, the Sagnac effect produces a shift $(\pm \Delta\omega_s/2)$ in the lasing CW and CCW angular frequencies (which at rest coincide at ω_0), where the beating frequency $\Delta \omega_s/(2\pi) = 4A\Omega/$ $(\lambda_0 L)$ depends on the angular velocity Ω of the rotating frame, the area A enclosed by the light path (of perimeter L) and on the emission wavelength, $\lambda_0 = 2\pi c/\omega_0$ (c, speed of light in vacuum). Evidently, the beating frequency $\Delta \omega_s/(2\pi)$ in this Hermitian setup (which is electronically detected) is always proportional to Ω and is dictated by geometrical constraints (Fig. 2b). The situation is entirely different for the non-Hermitian configuration, where the carrier angular frequency ω_0 can split by $\pm \Delta \omega_c/2$ even in the absence of rotation because of coupling effects arising from the scatterer (Fig. 2c). In this same static frame, by adjusting the differential loss Δy , these two resonances can fuse with each other once again at about ω_0 , thus marking the presence of an EP. After the system is set at an EP, upon rotation Ω , the Sagnac shifts $\pm \Delta \omega_s/2$ induce two new angular frequency lines at $\omega_0 \pm \Delta \omega_{FP}/2$ (Fig. 2c). In this case, the beating frequency $\Delta\omega_{\text{EP}}/(2\pi)$ is no longer proportional to Ω , but instead varies in an enhanced fashion because in this regime $\Delta\omega_{\rm EP} \propto \sqrt{\Omega}$, as expected when operating in the vicinity of an EP (Fig. 2c).

The frequency eigenvalues of the non-Hermitian RLG can be directly obtained from the transfer matrix T, after imposing periodic boundary conditions. From this, the induced non-Hermitian splitting $\Delta\omega_{\text{FP}}$ can be obtained, which interestingly enough remains unaffected even in the presence of gain saturation (see Supplementary Information). On the basis of these results, under rest conditions, one can compute the frequency split associated with the CW and CCW counter-propagating modes in our system as a function of the HWP angle when, for example, the coupling strength is set to $\kappa = 400$ kHz (Fig. 3a). In this case, an EP appears at $\beta \approx 4.7^{\circ}$. The corresponding magnitude of the complex eigenvalues $|\Lambda_{1,2}|$ of the system is plotted in Fig. 3b. The frequency beating signals expected from the Hermitian (orange line) and the non-Hermitian (black line) configurations of the RLG are plotted in Fig. 3c as a function of Ω . In the non-Hermitian case, we assume that the system is positioned at an EP ($\kappa = \Delta y$) when $\kappa = 400$ kHz. The EP enhancement of the Sagnac shift is evident in this figure. For these parameters, if, for example, the system rotates at $\Omega = 1^{\circ}$ s⁻¹, the Sagnac signal from the unmodified version of this RLG (Hermitian) is approximately 7.325 kHz, whereas the signal from the retrofitted (EP-based) system is expected to be about 5.2 times larger. Finally, Fig. 3d shows the change of beat note as a function of gyration speed when the system deviates from the EP (by 0.05% to 0.1% of the coupling strength). Although ideally one must keep the system at the EP, for small deviations the resulting error appears to be negligible.

Figure 4a depicts experimental results obtained from our non-Hermitian RLG system when it was biased at an EP. In our experiments, before each set of measurements performed, the system was positioned at an EP by monitoring the beat note as a function of the HWP rotation angle (gain-loss contrast), that is, setting the beat frequency as close as possible to zero. To do so, the HWP rotation angle was adjusted using a motorized rotation stage while the other components in the system

Article

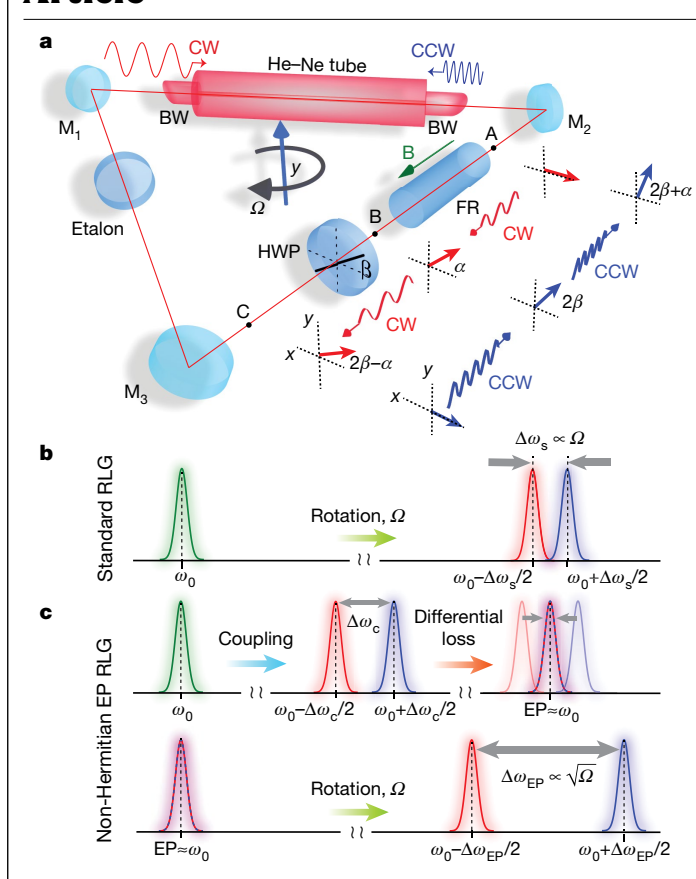


Fig. 2 | Principle of operation of an EP-based He-Ne RLG. a, The equilateral RLG cavity comprises three highly reflective mirrors (M₁, M₂, M₃), a He-Ne gas tube as the gain medium, and an etalon used to select the desired longitudinal mode(s). In contrast to a standard RLG, the EP-based cavity also includes a Faraday rotator (FR) and a half-wave plate (HWP). These two elements, in conjunction with the Brewster windows (BWs), introduce a differential loss between the clockwise (CW; A \rightarrow C) and counter-clockwise (CCW; C \rightarrow A) directions. **b**, In a standard RLG, the Sagnac effect induces a shift $(\pm \Delta \omega_s/2)$ in the stationary lasing angular frequencies (ω_0) associated with the CW and CCW modes. The resulting angular beating frequency $\Delta \omega_s$ is proportional to the angular velocity Ω of the rotating frame. \mathbf{c} , In an EP-based arrangement, the CW and CCW modes are first coupled to each other owing to the presence of weak scattering in the system. Consequently, the stationary lasing angular frequency (ω_0) splits according to the ensuing coupling strength $(\pm \Delta \omega_c/2)$. On the other hand, the loss contrast (Δy) induced by the simultaneous action of the FR, HWP and BWs brings the two split modes back to ω_0 , that is, to an EP. Once the RLG is biased at the EP, the gyration will lead to a beat frequency that is proportional to $\sqrt{\Omega}$. It is expected that for small rotation rates, the beat note of the EP-based RLG will be considerably enhanced in comparison to that of a standard arrangement.

were left intact. The figure provides data corresponding to three different coupling strengths, along with data from the standard unmodified RLG arrangement. These results are plotted in a log-log scale as a function of the rotation rate Ω for $\kappa = 65$ kHz, 150 kHz, 425 kHz. Whereas the response of the standard configuration is linear with respect to Ω (slope of 1), the same is not true for its non-Hermitian embodiment. In the latter case, the response is found to vary as the square root of the rotation rate Ω , as is evident from the slope of the accompanying three curves, which is very close to ½-a clear indication that an EP is at play. Our experimental observations clearly show that the scale factor of the Sagnac effect is substantially boosted by exploiting the very properties of EPs. The resulting Sagnac enhancement factors (with respect to the standard arrangement) are plotted in Fig. 4b for the same three cases. For $\kappa = 425$ kHz, a sensitivity boost of more than an order

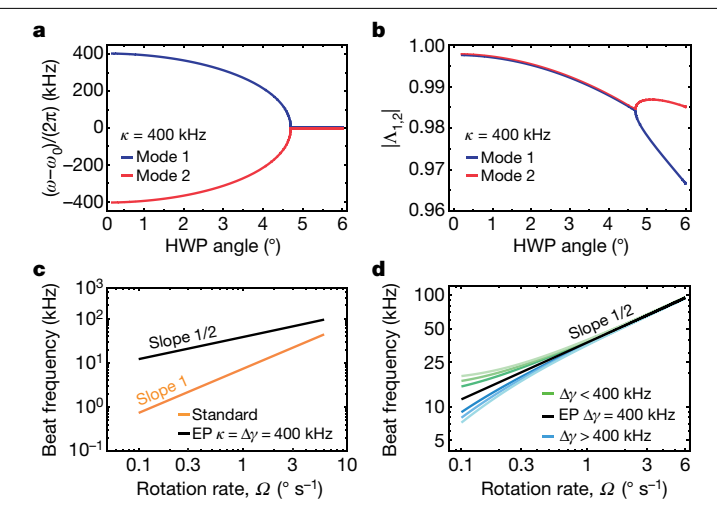


Fig. 3 | Bifurcations of complex eigenfrequencies and sensitivity enhancement of EP-based RLG around an EP. a, Resonance frequencies associated with the two coupled modes of an EP-based RLG at rest versus the HWP angle when the coupling strength κ is set to 400 kHz. These plots are obtained from Jones matrix analysis after considering gain saturation effects (see Supplementary Information, equation (16)). The EP in this system occurs at an HWP angle of about 4.7°. **b**, Magnitude of the same eigenvalues as a function of HWP angle when the non-Hermitian RLG is stationary (see Supplementary Information, equation (3)). \mathbf{c} , Beat frequency as a function of angular speed Ω (in log-log scale) for a standard RLG (orange) and a non-Hermitian RLG (black) (see Supplementary Information, equation (6)). The RLG is set exactly at the EP, where the loss contrast balances the coupling ($\Delta y = \kappa = 400 \text{ kHz}$). For the standard RLG, the slope of the curve is unity, whereas it is reduced to $\frac{1}{2}$ for the non-Hermitian arrangement. d, Calculated beat frequency for the non-Hermitian RLG as a function of rotation rate Ω (see Supplementary Information, equation (6)) when the loss contrast does not exactly balance the coupling (the differential loss differs from the coupling by 0.05%-0.1%) and hence the system is not precisely located at the EP. Whereas at large rotation rates the slope is approximately 1/2, it deviates from this value at small angular velocities when $\Delta \gamma \neq \kappa$. When $\Delta \gamma > \kappa$ (above the EP) the beat frequency (blue lines) is below that of the ideal case (black line), which indicates a reduced sensitivity to the rotation Ω . On the other hand, when the system is biased below the EP ($\Delta y < \kappa$), the beat frequency does not exhibit a strong dependence on the gyration speed.

of magnitude is observed when $\Omega = 0.4^{\circ} \, \text{s}^{-1}$. The reported minimum gyration speed, $\Omega = 0.1^{\circ} \, \text{s}^{-1}$, is imposed by the limited rotation capability of the apparatus. The estimated rotation rate is obtained from the beat frequency by applying the transfer functions associated with the Hermitian and non-Hermitian arrangements. These transfer functions are illustrated in Fig. 5a, where it can be observed that for small angular velocities, not only the absolute value of the beat frequency $(\Delta v_{\rm FP} > \Delta v_{\rm S})$; where $\Delta v_{\rm FP} = \Delta \omega_{\rm FP}/(2\pi)$ and $\Delta v_{\rm S} = \Delta \omega_{\rm S}/(2\pi)$ is the rotationinduced beat frequency in the EP-based RLG and the standard RLG, respectively) increases dramatically for the EP-based system, but also an incremental step in the rotation rate is transferred to a much larger difference in the beat frequency ($|\Delta v_{EP,2} - \Delta v_{EP,1}| > |\Delta v_{S,2} - \Delta v_{S,1}|$). As a result, the resolution of the estimated rotation speed is potentially improved. Figure 5b, c displays the error bars on the estimated rotation rates, as obtained experimentally for the Hermitian and non-Hermitian arrangements, respectively. In a standard gyroscope, the relationship between the applied and estimated angular velocities is linear. On the other hand, owing to the nonlinear transfer function associated with the non-Hermitian system, these two quantities are not on an equal footing anymore. In this respect, only when considering the nonlinearity of the transfer function, the errors on the estimated rotation rate can be interpreted correctly. Consequently, at higher rotation speeds, the modified gyroscope displays larger error bars, as shown in Fig. 5c.

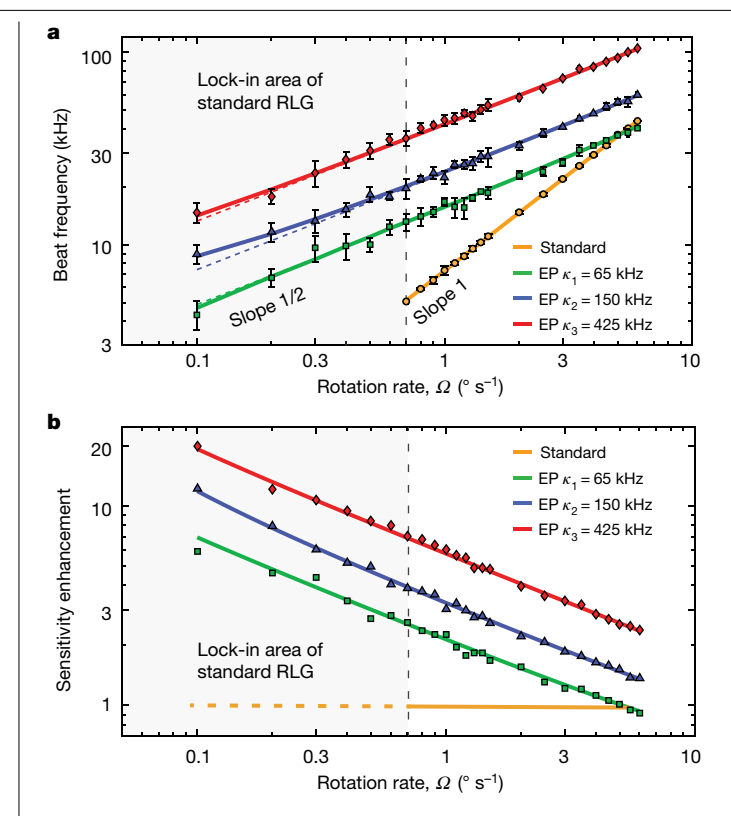


Fig. 4 | Measured beat frequency and sensitivity enhancement factor versus **rotation rate. a**, Beat frequency versus rotation rate Ω (in log-log scale) for a standard RLG (orange data marks) and a non-Hermitian RLG at three different coupling strengths, $\kappa_1 = 65 \,\text{kHz}$ (green), $\kappa_2 = 150 \,\text{kHz}$ (blue) and $\kappa_3 = 425 \,\text{kHz}$ (red). The dashed lines correspond to theoretical calculations in which the non-Hermitian system is biased exactly at the EP $(\Delta y_i = \kappa_i)$. The solid lines represent fitted data obtained when the system is slightly detuned from the EP (see Supplementary Information, equation (11)) (here $\Delta y_1 = 1.0003 \kappa_1$, $\Delta v_2 = 0.9992 \kappa_2$, $\Delta v_3 = 0.9999 \kappa_3$). The orange line has a slope of unity, indicating that the Sagnac shift in the standard cavity varies linearly with Ω . By contrast, the slope associated with the non-Hermitian curves is approximately 1/2, indicating the presence of an EP. Moreover, whereas in the standard RLG the lock-in effect limits gyration measurements below $\Omega = 0.7^{\circ} \, \text{s}^{-1}$ (shaded region), the EP-based configuration is capable of detecting smaller rotation rates (only limited by the resolution of the step motor, $0.1^{\circ}\,\mathrm{s}^{-1}$). The error bars show one standard deviation from the mean of the collected data. b, The sensitivity enhancement, defined as the ratio of the non-Hermitian beat frequency to that of a standard RLG, is obtained from the measured data for the aforementioned three coupling strengths. For $\Omega < 0.7^{\circ} \, \text{s}^{-1}$, the sensitivity enhancement is calculated using the anticipated value of the beat frequency from the standard RLG, provided that lock-in does not occur. The solid lines (red, blue and green) represent theoretical curves corresponding to the parameters used in our experiments.

The advantage of the EP-based gyroscope becomes apparent at smaller velocities, where the error in the estimated rotation rates decreases rapidly. This is depicted in Fig. 5b, c, where a noise component of 3 kHz has been added to the ideal system (shown as orange and red shaded regions).

Several factors must be considered when using non-Hermitian arrangements for sensing purposes. First and foremost is appreciating the difference between sensitivity and detection limit²⁵. In non-Hermitian settings, the sensitivity enhancement is a fundamental feature that is dictated by mathematical properties, governed by the perturbation expansion around an EP. The detection limit, on the other hand, depends on the physical system and is primarily determined by the net gain (or loss), as well as the correlation between the laser noise associated with the two resonances^{26,27}. In this regard, one in principle

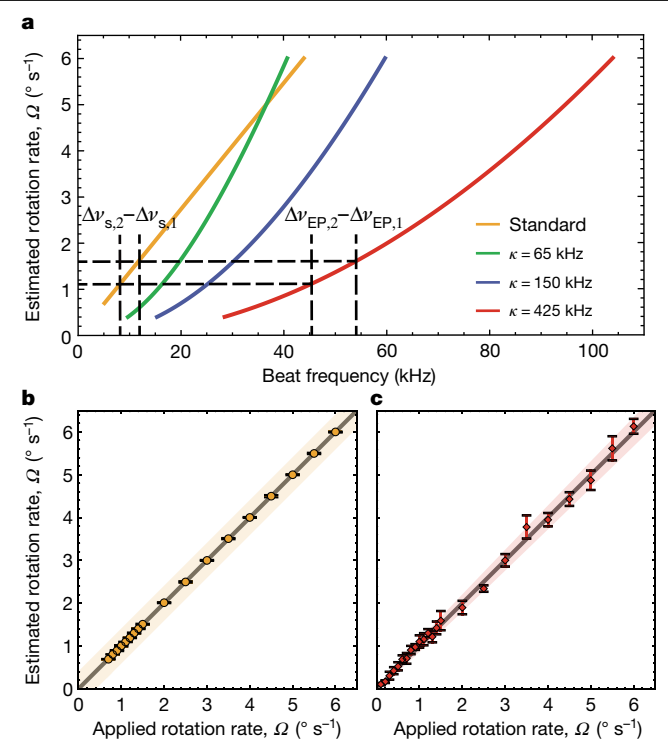


Fig. 5 | Transfer functions and estimated rotation rates. a, The transfer function of the standard system (orange line)—that is, its response to a beat frequency—is compared to that of the EP-based RLG for $\kappa = 65, 150, 425 \,\mathrm{kHz}$ (green, blue and red lines, respectively). For the non-Hermitian gyroscope, at small rotation rates both the absolute values of the beat frequency $(\Delta v_{\rm FP} > \Delta v_{\rm S})$ and of the beat frequency differences $(|\Delta v_{EP,2} - \Delta v_{EP,1}| > |\Delta v_{S,2} - \Delta v_{S,1}|)$ for an incremental step in the rotation rate increase dramatically, b, c, Predicted rotation rate for the standard RLG (b) and for the modified non-Hermitian RLG at $\kappa = 425$ kHz (c), obtained by applying the associated transfer functions to the measured beat frequencies. The shaded areas demonstrate the effect of noise (3 kHz) on the estimated rotation rates. The error bars show one standard deviation from the mean of the collected data.

can increase the net gain while keeping the RLG at the EP by managing the gain contrast to boost both the sensitivity and the detection limit—as we did in our design. As expected from the Schawlow-Townes formula, an increase in the net (average) gain of the system (or the output power) will reduce the linewidth of the laser. This in turn tends to compensate for the linewidth broadening near the EP while allowing one to exploit the larger sensitivity afforded by such singularities. Another technical issue is how closely one can reach and stabilize the system at the $\mathsf{EP}^{28,29}.$ In our experiment, we fully rely on positioning the RLG at the EP before each set of measurements, by visually monitoring the beat note as a function of the HWP rotation angle (gain-loss contrast). In future devices to be used in the field, one may need to actively control the system to remain biased at the EP. Such approaches have been suggested elsewhere 11,30.

In conclusion, we have demonstrated for the first time, to our knowledge, a new class of non-Hermitian RLGs that can display an enhanced Sagnac sensitivity. This is accomplished by exploiting the intriguing properties of a special family of non-Hermitian spectral singularities, the EPs. At these points, the RLG response has a square-root dependence on the gyration speed, in contrast to the linear response observed in standard arrangements. The proposed configuration may inspire new technological developments in various settings in which measuring low rotation rates via ultracompact systems is highly attractive. Finally, the idea of transforming a standard measuring apparatus into an EP-based device with superior sensitivity may have important ramifications in other areas of science and technology.

Article

Online content

Any methods, additional references. Nature Research reporting summaries, source data, extended data, supplementary information, acknowledgements, peer review information; details of author contributions and competing interests; and statements of data and code availability are available at https://doi.org/10.1038/s41586-019-1780-4.

- Armenise, M. N., Ciminelli, C., Dell'Olio, F. & Passaro, V. M. Advances in Gyroscope Technologies (Springer, 2010).
- Post, E. J. Sagnac effect. Rev. Mod. Phys. 39, 475-493 (1967).
- Chow, W. W. et al. The ring laser gyro. Rev. Mod. Phys. 57, 61-104 (1985).
- Macek, W. M. & Davis, D. T. M. Jr Rotation rate sensing with traveling-wave ring lasers. Appl. Phys. Lett. 2, 67-68 (1963).
- Boyd, R. W. Slow and fast light: fundamentals and applications. J. Mod. Opt. 56, 1908-1915 (2009).
- Shahriar, M. S. et al. Ultrahigh enhancement in absolute and relative rotation sensing 6. using fast and slow light. Phys. Rev. A 75, 053807 (2007).
- Smith, D. D., Chang, H., Arissian, L. & Diels, J. C. Dispersion-enhanced laser gyroscope. 7. Phys. Rev. A 78, 053824 (2008).
- Kaplan, A. E. & Meystre, P. Enhancement of the Sagnac effect due to nonlinearly induced 8 nonreciprocity. Opt. Lett. 6, 590-592 (1981).
- 9 Hodaei H et al Enhanced sensitivity at higher-order exceptional points. Nature 548 187-191 (2017); erratum 551, 658-191 (2017).
- Chen, W., Özdemir, Ş. K., Zhao, G., Wiersig, J. & Yang, L. Exceptional points enhance sensing in an optical microcavity. Nature 548, 192-196 (2017).
- Ren, J. et al. Ultrasensitive micro-scale parity-time-symmetric ring laser gyroscope. Opt. Lett. 42, 1556-1559 (2017).
- Sunada, S. Large Sagnac frequency splitting in a ring resonator operating at an exceptional point. Phys. Rev. A 96, 033842 (2017)
- Grant, M. J. & Digonnet, M. J. F. Loss-gain coupled ring resonator gyroscope. In Proc. SPIE Optical, Opto-Atomic, and Entanglement-Enhanced Precision Metrology Vol. 10934 (SPIE, 2019).
- Vahala, K. J. Optical microcavities. Nature 424, 839-846 (2003).

- Vollmer, F. & Arnold, S. Whispering-gallery-mode biosensing: label-free detection down to single molecules. Nat. Methods 5, 591-596 (2008)
- Lu, T. et al. High sensitivity nanoparticle detection using optical microcavities. Proc. Natl Acad. Sci. USA 108, 5976-5979 (2011).
- Liang, W. et al. Resonant microphotonic gyroscope. Optica 4, 114-117 (2017)
- Makris, K. G., El-Ganainy, R., Christodoulides, D. N. & Musslimani, Z. H. Beam dynamics in PT symmetric optical lattices. Phys. Rev. Lett, 100, 103904 (2008).
- Klaiman, S., Gunther, U. & Moiseyev, N. Visualization of branch points in PT-symmetric waveguides. Phys. Rev. Lett, 101, 080402 (2008).
- Moiseyev, N. Non-Hermitian Quantum Mechanics (Cambridge Univ. Press, 2011).
- Wiersig, J. Enhancing the sensitivity of frequency and energy splitting detection by using exceptional points: application to microcavity sensors for single-particle detection. Phys. Rev. Lett. 112, 203901 (2014).
- El-Ganainy, R. et al. Non-Hermitian physics and PT symmetry. Nat. Phys. 14, 11-19 (2018).
- Yariy, A. & Yeh, P. Photonics: Optical Electronics in Modern Communications (Oxford Univ. Press, 2006).
- Khajayikhan, M., John, K. & Leger, J. R. Experimental measurements of supermodes in superposition architectures for coherent laser beam combining, IEEE J. Quantum Electron, 46, 1221-1231 (2010)
- Hu, J., Sun, X., Agarwal, A. & Kimerling, L. C. Design guidelines for optical resonator biochemical sensors. J. Opt. Soc. Am. B 26, 1032-1041 (2009).
- LIGO Scientific and Virgo Collaboration. GW170104: observation of a 50-solar-mass binary black hole coalescence at redshift 0.2. Phys. Rev. Lett. 118, 221101 (2017).
- Collett, M. J., Loudon, R. & Gardiner, C. W. Quantum theory of optical homodyne and heterodyne detection. J. Mod. Opt. 34, 881-902 (1987).
- Mortensen, N. A. et al. Fluctuations and noise-limited sensing near the exceptional point of parity-time-symmetric resonator systems. Optica 5, 1342-1346 (2018).
- Zhang, M. et al. Quantum noise theory of exceptional point amplifying sensors. Phys. Rev. Lett. 123, 180501 (2019).
- De Carlo, M., De Leonardis, F. & Passaro, V. M. Design rules of a microscale PTsymmetric optical gyroscope using group IV platform. J. Light. Technol. 36, 3261-3268

Publisher's note Springer Nature remains neutral with regard to jurisdictional claims in published maps and institutional affiliations.

© The Author(s), under exclusive licence to Springer Nature Limited 2019

Data availability

All data that support the findings of this study are available within the paper and the Supplementary Information and are available from the corresponding author upon reasonable request.

Acknowledgements We acknowledge support from the US Air Force Office of Scientific Research (FA9550-14-1-0037), Office of Naval Research (N00014-16-1-2640, N00014-18-1-2347, N00014-19-1-2052), National Science Foundation (ECCS1454531, DMR-1420620, ECCS1757025), Army Research Office (W911NF-16-1-0013, W911NF-17-1-0481), US-Israel Binational Science Foundation (BSF) (2016381), DARPA (D18AP00058, HR00111820042, HR00111820038) and the European Commission Project 'Non-Hermitian Quantum Wave Engineering' (NHQWAVE, MSCA-RISE 691209). We thank W. Luhs for help in setting up the

gyroscope and for performing some of the initial measurements, S. Milady, S. Rotter and K. Vahala for technical discussions, and S. Rotter for supporting this project through funding for A.S.

Author contributions All authors contributed equally to this work.

Competing interests The authors declare no competing interests.

Additional information

Supplementary information is available for this paper at https://doi.org/10.1038/s41586-019-1780-4

 $\textbf{Correspondence and requests for materials} \ should \ be \ addressed \ to \ M.K.$

Peer review information *Nature* thanks Chia Wei Hsu and the other, anonymous, reviewer(s) for their contribution to the peer review of this work.

Reprints and permissions information is available at http://www.nature.com/reprints.